

Dealing with unique minerals in petrophysical logs

Munish Kumar ^{a,*}, Ryan Isaac Lazaroo ^b

^a Singapore University of Social Sciences, Singapore

^b Nanyang Technological University, Singapore

ARTICLE INFO

Keywords:

Opalines
Volcanics
Tuffs
Opal-CT
Petrophysics
Russian-logs

ABSTRACT

Most petrophysical equations and methods are designed to deal with hydrocarbons found within mineralogies, such as quartz and feldspars or calcite and dolomite. Petrophysical tools and techniques have also largely been designed to investigate rocks containing these minerals. Hence, when log analysts encounter a field containing unique mineralogies, determining an appropriate petrophysical evaluation process for such unconventional reservoirs can be a challenge. In this paper, we aim to discuss our learnings using two unique case studies. The first is a well which had intersected opalines and logged with conventional modern “western style” tools. The second is a well which has intersected tuffs and volcanics and which was logged with older “Russian style” tools.

For opalines, we discuss the potential mineral signatures observed on the well log data and the reservoir potential of the rocks. We find that the unique microporous structure created by opal-CT microspheres/lepispheres, combined with either fracture or matrix-porosity dominant properties, potentially allows for storage of hydrocarbons within the rock. Hence, we hypothesize that opaline reservoirs could be classed as “Low Resistivity Low Contrast” (LRLC) pay and should not be glossed over just because typical hydrocarbon indicators are not seen.

For tuffs and volcanics, we first share some of the challenges faced and methods used in conducting modern petrophysical interpretation with data from older Russian-style logs. Again, we discuss the potential mineral signatures observed on the logs and look at properties such as pore throat radii, size, and mineral composition and how that affected reservoir potential. Our findings indicate that the distribution of pore sizes allowed for greater connectivity within the rock, where the pore geometry effects aided in low residual oil saturations.

One-sentence summary

This paper aims to discuss the petrophysical considerations that need to be made for unique mineralogy that is sometimes seen in logs, like tuffs and opalines.

1. Introduction

Most petrophysical models are built with an understanding that the most hydrocarbon deposits are found in basins that have an underlying mineral system that is sedimentary in nature. These sedimentary basins are primarily composed of minerals that are either silicates ($[SiO_{4-x}^{4-2x}]_n$), such as quartz, feldspars, micas and other clays, or carbonate (CO_3^{2-}) (calcite and dolomite), and while the nature of the petrophysical properties and reservoir type are very much dependent on the environment of deposition and can vary across sedimentary basins

(homogeneous, heterogeneous, tight, layered or laminated), our main petrophysical equations are designed to deal with these commonly encountered minerals. However, we know from both individual as well as collective industrial experience that there are instances where unique minerals are encountered in fields drilled around the world.

In Indonesia (Winardi et al., 2021), Australia (Ellis, 2016), and Egypt (Nabawy et al., 2022) for instance, pyritic sandstones are encountered in some hydrocarbon bearing reservoirs. These have some interesting effects on the logs, from having high densities to low resistivity responses. Kennedy and Clavier et al. both discussed the impact of pyrite (FeS_2) on modern logs (Clavier et al., 1976; Kennedy, 2004) and noted that pyrite has a variety of effects on resistivity and nuclear tools, such that measured values can be drastically different from those typically encountered. One phenomenon that can be caused by the presence of conductive minerals such as pyrite or glauconite is low resistivity-low contrast (LRLC) pay. This is when typically high resistivity hydrocarbon zones in between shales are bypassed through means such as

* Corresponding author.

E-mail address: munishkumar001@suss.edu.sg (M. Kumar).

conductive minerals, resulting in low resistivity readings throughout the sequence and resulting in missed pay opportunities (Pratama et al., 2017). These same authigenic minerals are also associated with reduced reservoir quality, for example in New Zealand (Radwan et al., 2021), further complicating the characterization of zones containing these unique minerals.

In the Gulf of Mexico (GOM) (Fredrich et al., 2007), in fields offshore Brazil (Armelenti et al., 2021), Egypt (Ali Ali, Emad El Din Abd Elrazik, Shebl Azam and Ahmed Hassan, 2016), and Algeria (Baouche and Nabawy, 2021), evaporite salts (halite, anhydrite, and sylvite) layers can overlie depositional basins or be present within producing reservoirs. While salt acts as an excellent sealing facies, due to its non-net nature with its very low porosity and permeability, salt encountered in reservoir sands has a deleterious effect on logs; resistivities can be very high (due to a lack of accessible pore space), density is well constrained since minerals are pure, with either very high or low values dependent on the elements present, and neutron can be either very high or very low dependent again on the nature of the salt type (Marisa, et al., 2018).

Some minerals encountered in hydrocarbon bearing reservoirs result in missed pay opportunities as in the case of LRLC pay mentioned earlier, and/or can appear as non-net sands if higher potassium (K), thorium (Th), or uranium (U) contents are not properly accounted for (hot sands). The Northern Carnarvon Basin in Australia, for example, contains reservoir sands in the Mungaroo Formation which are glauconitic in nature (Feng et al., 2020). Glauconite is an iron rich clay variety, and is ductile and compacts under overburden conditions, potentially occluding primary porosity. Properly accounting for glauconite in a reservoir firstly requires an understand of the microporous nature of the glauconite particle itself. Hot sands are present in the Tenggol Arch, offshore east Peninsular Malaysia and are characterized by higher gamma ray (GR) signature associated with Th. This needs to be accounted for, otherwise the evaluation of clay proportions would be incorrect, resulting in an underestimation of net sand. The accounting of the hot sand components also allows for the proper correlation across wells at the field scale (Jong et al., 2019).

In all the above examples, literature adequately describes how such reservoirs should be dealt with. In almost all cases, the fundamental petrophysical equations derived for volume of shale (VSH), porosity (ϕ) and saturation (S_w) will apply, so long as appropriate corrections/calibrations are used. There are exceptions to the rule, however. If salt, for example, is encountered in a continuous zone but deposited as its own layer, then petrophysicists may choose to either treat the zone as non-net and not interpret or adopt a simplistic but consistent method, given that there are no set standard industry equations. In this case, the interpretation goal is not to determine salt properties, but rather to allow for comparison across large areas with salt bearing intervals, and to avoid interpreter bias. A simplistic method could be VSH from GR, total porosity from nuclear magnetic resonance (if available), density or sonic (but with consistent end points) and S_w set to 1. If there is salt present as pore filling material, then adopting an interpretation method as described by Saxena and McDonald is perhaps the way to go (Saxena and McDonald, 2009). However, for some even less encountered mineralogies, there are few if not no standard interpretation methods to be found within existing literature and hence much uncertainty in how to handle them.

In this paper we will discuss, via two separate case studies of less encountered mineralogies, some of our experiences and interpretation methods in dealing with unique situations observed in our work and how they are quantified for petrophysical applications. We will discuss wells that have intersected (a) opalines and (b) volcanics (tuffs). We will explain how we have addressed such petrophysical challenges and discuss which tools are perhaps the most reliable in discriminating potential mineral signatures.

2. Case study 1: Opalines

2.1. Background

Opaline rocks are named as such because they contain opal, a hydrated silica mineraloid which can form in hydrothermal springs, volcanic, and marine environments. They can also be biogenic in nature as in the case of diatomite. Opals have multiple forms and phases and are typically classified as having amorphous (opal-A), ordered Cristobalite (opal-C), or disordered Cristobalite and Tridymite (opal-CT) structures (Jones and Segnit, 1971). The amorphous opal-A lacks a crystalline structure. With increasing diagenesis, opal-A morphs into a more stable paracrystalline opal-CT which contains layers of intergrowth and displays characteristics of both cristobalite and tridymite (Curtis et al., 2019). With time, these opals turn into quartz, the most stable of the silica polymorphs. Across all these transitions, the petrophysical properties of the rocks change significantly and hence opalines encompass a wide range of characteristics.

This range of petrophysical characteristics is important in determining the role of opalines in hydrocarbon storage, where they can act as both reservoirs and seals. In terms of reservoir potential, opaline rocks can be characterized by their high porosity which makes it possible to store hydrocarbons (Derkowski et al., 2015). The porosity can drop from above 55% in opal-A to about 25% in opal-CT, and permeabilities drop from an already low <10 mD to negligible levels in opal-CT and quartz (Chaika and Dvorkin, 2000; Reid and McIntyre, 2001). However, these opal-CT and quartz reservoirs still have potential to store hydrocarbons, as displayed in the Monterey Formation of Elk Hills Field in California and Yurihara Field in Japan, where such reservoirs have proven to produce (Reid and McIntyre, 2001; Tsuji et al., 2011). Chaika and Williams (2001) have also classified these types of siliceous reservoirs into two groups – Matrix porosity-dominated (Group 1) as in previous examples, and fracture-dominated. Their study shows the importance of being able to recognize the two different groups of opalines in better evaluating the reservoir potential of a field.

The low permeability of opalines also allow them to act as seals which trap hydrocarbons, given the right composition and conditions. This was seen in the Yurihara Field in Japan, where the less porous and less permeable clay-rich opal-CT seals in hydrocarbons within the more permeable quartzose porcelanites below. However, in shallower sections of opal-CT, confining pressure was not sufficient and permeabilities increased to values similar to the underlying quartzose porcelanites, allowing hydrocarbons to escape (Tsuji et al., 2011). There is also the possibility of tectonic-induced fracturing that may break the reservoir seals given the more brittle nature of opalines compared to other common seal rocks.

The storage or sealing capabilities of opalines may also be affected by several other factors. One such factor is the clay content of the opalines. Tsuji et al. (2011) find that higher clay content can make opalines better seals, while lower clay content improves their reservoir potential. Lithology of the opalines can also determine how brittle the reservoir can be, for example opaline chert can be much more fractured than opaline porcelanite (Reid and McIntyre, 2001). Lastly, the differences in response to heat between opal-A and opal-CT means that when using steam injection in the extraction of hydrocarbons, opal-A becomes less permeable, and this makes opal-CT a more equally viable option despite normally having lower permeabilities than opal-A (Dietrich, 2017).

Overall, the existing literature suggests that there is no one defined course of action in evaluating the reservoir potential of opalines, owing to their wide range of types and characteristics. At the same time, all three main types of opal have shown promise in their ability to act as producing reservoirs and hence should not be glossed over without more careful examination in logs. In the following sections, we document our approach to examining the hydrocarbon potential of a well which had penetrated opalines.

2.2. Case study parameters and setting

At a recently concluded drilling campaign in 2017, an opaline rich reservoir was penetrated about 200 km off the coast of South America. The drilled well, Well DS, was located in waters over 1000 m deep, on a transform marginal plateau. Regional stratigraphy ranges from deep marine clastic deposits to shallow marine and shelfal carbonates formed in a series of transgressive-regressive cycles, with several major and minor unconformities found within the stratigraphy formed by relative sea level changes. Well DS had met the pre-drill expectations of a thick net reservoir in a four-way closure having good porosity, characterized by a brightening on the seismic amplitudes. However, upon logging and core sampling, the well was found to have penetrated non-reservoir quality limestones, shales, and opaline porcelanites – the last of which is the focus of this study.

Evidence of hydrocarbon presence in Well DS came in the form of a collected gas sample downhole, in addition to observed hydrocarbon effects on the density and neutron logs within the well. The well was therefore defined as a technical success as it proved the existence of a producing source rock, migration, and suitable timing.

2.3. Approach

The distribution of opal in the reservoir rocks can be heterogeneous. Additionally, since it shows up as a bright amplitude on seismic due to its highly porous nature, there is a need to study its overall effect on the raw log measurements and use that as calibration parameters to support seismic-driven exploration campaigns. This was the goal of the analysis of the opaline reservoir in Well DS; an evaluation of its concentration, distribution in the reservoir (vertically and horizontally) and concentration which could improve quantitative analysis and de-risk other potential opportunities.

2.4. Interpretation results - well DS

A set of basic logs (GR, RES and D-N) (see Fig. 1) as well as core samples are present in Well DS. The effect of opal on the logs is varied; it

is observed that opaline has a smaller effect on sonic and neutron logs but has a larger effect on the density log. This large effect is best explained in Fig. 2, which shows the significantly lower grain densities of opaline samples (~ 2.2 g/cc) compared to the sandstone and limestone intervals (2.6–2.72 g/cc). Note that while the lower density value of opaline in this sample is attributed mainly to a microporous structure, it could also be due to dissolution and leaching of microfossils or possibly fractures. Both photoelectric effect (PEF) and bulk density correction (DRHO) logs do not show significant anomalous values; DRHO is $\sim 0.058 \pm 0.012$ g/cc and PEF is $\sim 3.73 \pm 0.79$. As the well was wet, the effect on resistivity is unclear, but given its microporous nature, resistivity suppression is very possible.

A series of core measurements done on collected sidewall core samples in Well DS, which showed that samples had good porosity, ranging from 25 to 41%. The permeability, while low at <10 mD, were in line with analogs found elsewhere. These values are distinct from the sandstone and limestone intervals from other wells in the area (Fig. 4)

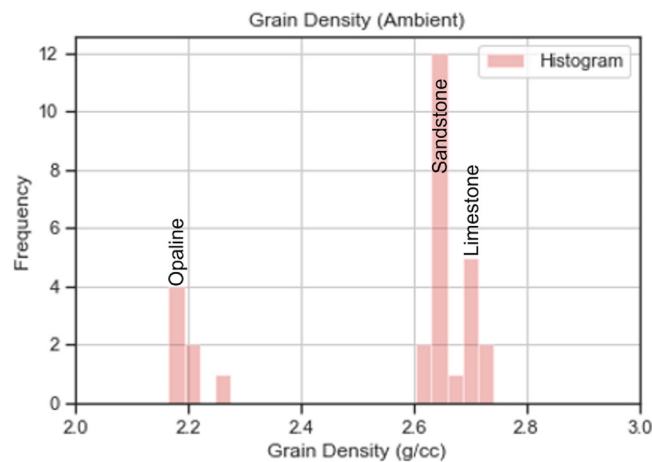


Fig. 2. Histogram of grain densities of samples from the same field as Well DS.

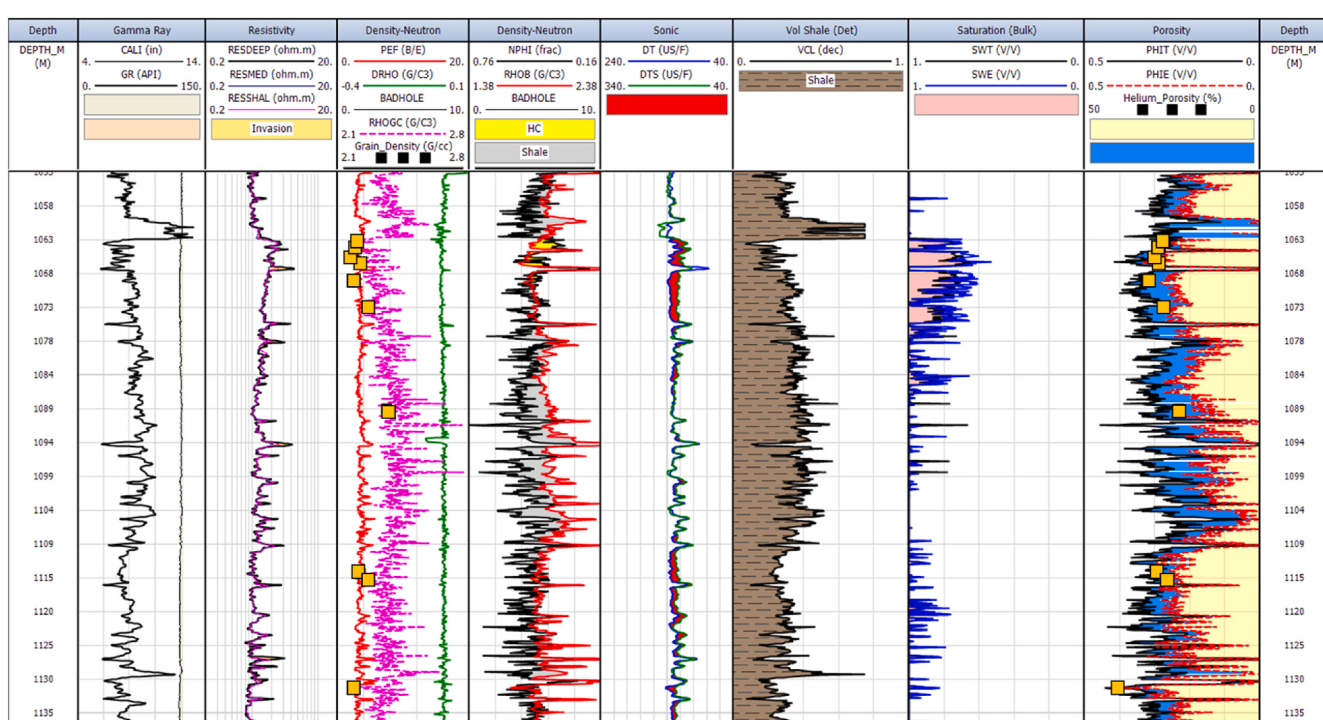


Fig. 1. Logs from well DS

and match up well to the porosities and permeabilities of opalines published in existing literature (Reid and McIntyre, 2001; Tsuji et al., 2011). The samples plot in the same region as opal-CT porcelanites from Tsuji et al. which is consistent with the classification of our samples.

Interestingly, Well DS sample points appear to lie firmly on the 'Group 2' trendline proposed by Chaika & Williams, suggesting a fracture-dominated reservoir (Fig. 5). However, based on thin sections and SEM images (Fig. 3), Well DS samples hold a degree of matrix porosity through micropores, while fractures do not readily show up in these sample. The characterization may still be accurate as it is possible that the limited Well DS samples do not fully capture the extent of fracturing within the opal-CT reservoir, as analog reservoirs with the same lithology have shown presence of microfractures throughout porcelanite layers (Reid and McIntyre, 2001).

For the petrophysical interpretation, we have firstly spliced, and depth aligned the logs. Environmental corrections are a challenge as the minerals are unique, but because the borehole is in good shape, we have assumed that the environmental corrections as provided by the logging contractor is generally adequate. From the gamma ray (GR), we observe that opaline has a highly variable GR signature, with values ranging from 30 to 90 GAPI. We attribute this to variable interspersed clay content in the depth interval. Resistivity shows no invasion effect but shows high resistivity spikes associated with cemented intervals. Overall, however, the resistivity response is fairly lazy and does not show significant variation throughout. There are intervals where the resistivity is higher, which we note to be related to the presence of higher porosities potentially. Interestingly, there is an interval from 1063 to 1068 mMD, where the resistivity is the highest. From 1068 to 1078 mMD, there also appears to be a "transition zone like" behavior. When viewed in connection with the density-neutron (RHOB-NPHI), this same zone shows a "hydrocarbon effect" (cross-over) which disappears as one goes deeper. The same "hydrocarbon effect" is also observed when an overlay of the compressional and shear sonic is viewed. We show a cross-plot of RHOB and NPHI and RHOB-PEF in Fig. 7.

In this well, we observe from the cross-plot that points lie somewhere between the limestone-dolomite trendline, although at the tail ends where porosities are high. Our recommended approach is to therefore interpret the well as you would a conventional petrophysical analysis, but with properly applied calibration to account for the extremely high porosities. We evaluate volume of shale (VSH) as a minimum of the GR and RHOB-NPHI, followed by the evaluation of volume of clay (VCL). From the ternary diagram in Fig. 8, we determine the average clay content to be ~50% and apply this as a multiplier to VSH.

Porosity is interpreted using RHOB-NPHI, with grain density calibrated to the core data. Note that the core data has an average grain density of 2.2 g/cc; however, we use values of between 2.1 and 2.3 g/cc depending on the interval. We adjust the values such that we have a match between interpreted grain density (RHOGC, track 4 from the left) and core-based grain density (black squares in track 4 from the left). Still, our match between total porosity (PHIT, track 2 from the right) and core porosity (black squares in track 2 from the right) is sometimes less than perfect.

For instance, while our core grain density is seen to be properly calibrated, our porosities show a slight mismatch from 1063 to 1068 mMD. In other intervals, however, the match is very good. We attribute this to challenges with getting accurate porosity measurements in opaline rich cores, as well as inaccuracies in the log measurements. As opal is essentially microporous in nature, core cleaning, drying, and therefore measurement of porosity/permeability can sometimes be inaccurate. Similarly, as mentioned previously, environmental corrections to such intervals are difficult. However, in general, we note that PHIT and core porosity follow a similar trend.

For saturation, we use dual water as the preferred method, but only to account for the clay effects, more than the opaline presence. We note there is hydrocarbons interpreted from 1063 to 1078 mMD. However, there is no pressure or samples at this depth to prove if this is mobile in any way.

2.5. Discussion

The unique porous microstructure of opaline as observed from Figs. 3 and 6, as well as the observation of fracture or matrix dominated properties (Fig. 5) means opaline reservoirs could potentially be classified as "Low Resistivity Low Contrast (LRLC) Pay". While Well DS did not have any definitive evidence of hydrocarbons and existing literature does not cover the behavior or mechanisms behind the potential of opalines as LRLC pay, the observations made of the microstructure for the well above is very similar to those made in sandstones and carbonate reservoirs elsewhere which have LRLC characteristics (Ashqar, 2016; Ayadiuno, 2017; Belevich, 2017; Boyd et al., 1995). Most LRLC wells have been characterized as low resistivity, high fluid saturation, but good hydrocarbon flow/production. The typically responses of resistivity can be from 1 to 5 ohmms (Worthington, 2000), which aligns with values of resistivity previously found in high opal-CT content reservoir rocks (~5 ohmms) (Reid and McIntyre, 2001). LRLC pay occurs when the absolute value of the resistivity is so low that pay zones are

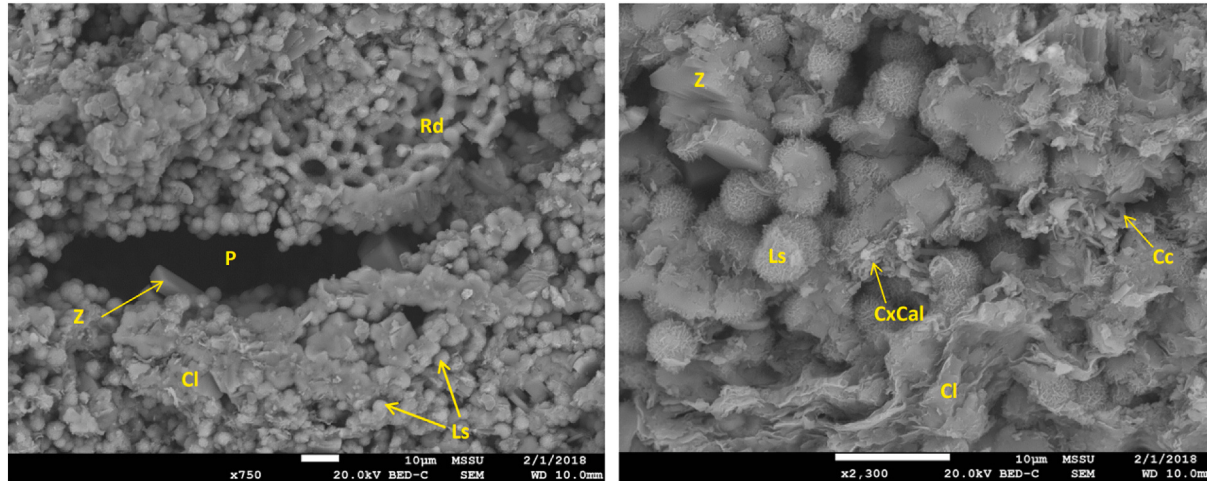


Fig. 3. Scanning Electron Microscope (SEM) images from Well DS. **Left:** An elongate pore (P) hosting zeolite crystals (Z) within the microporous smectitic-illitic clay (Cl) and opal lepisphere (Ls) matrix. Intraparticle porosity is also found within a radiolarian (Rd) fragment. **Right:** Close up of a typical microporous matrix of flaky detrital smectitic-illitic clay (Cl) and opal lepispheres (Ls). Contains scattered zeolite crystals (Z), cryptocrystalline calcite (CxCal), and coccoliths (Cc).

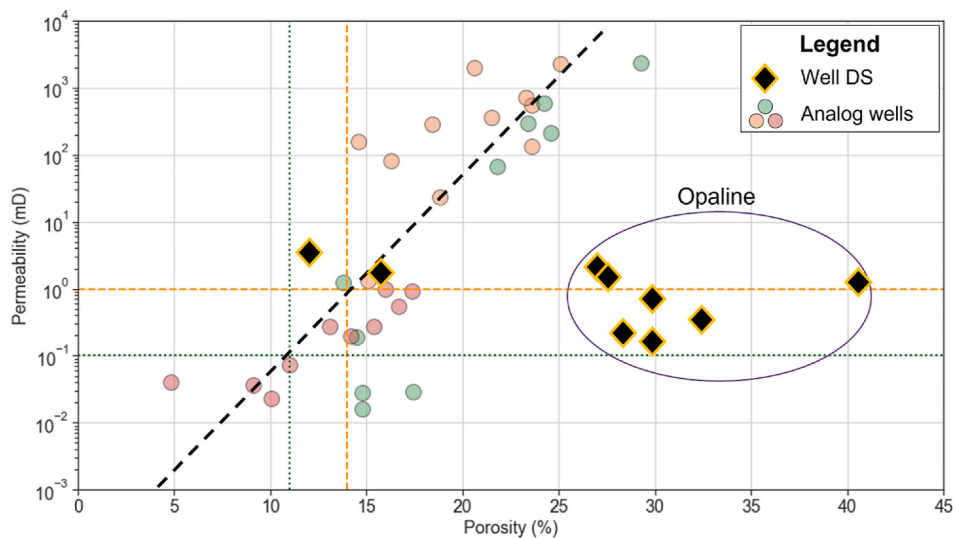


Fig. 4. Cross-plot of permeability and porosity for Well DS and analog wells.

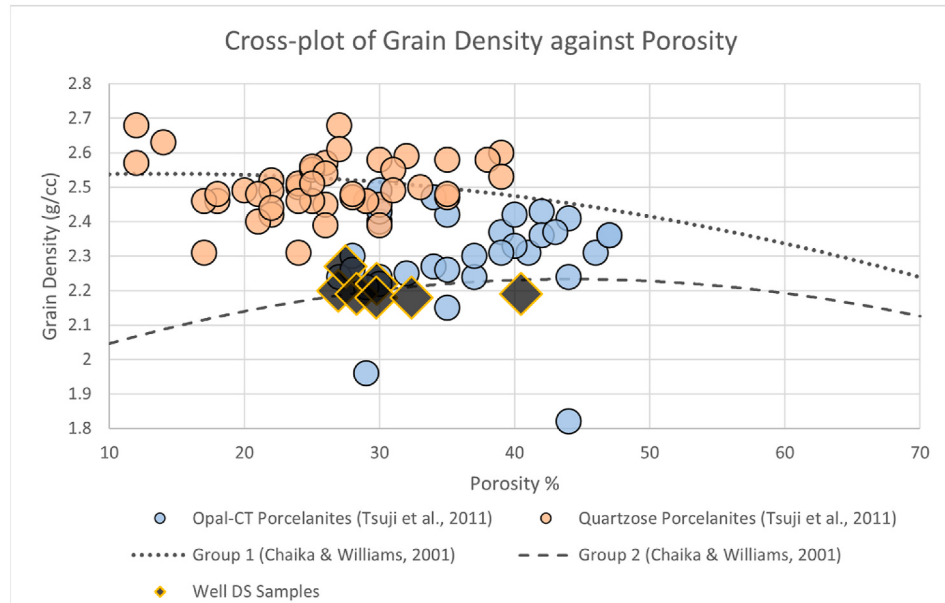


Fig. 5. Cross-plot of grain density and porosity for various samples, including Well DS. Adapted from [Tsuji et al. \(2011\)](#).

overlooked. LRLC pay can occur where the water saturation as calculated from the resistivity is incorrect and overestimates the true water saturation of the formation. The issue is then to find improved methods for calculating the true water saturation, either by modification of the calculation algorithm used from the resistivity, or possibly by obtaining saturation data by an alternative and independent means. Either scenario involves an understanding of why the water is effectively not mobile, and to develop some means for predicting which rocks will flow dry hydrocarbons and which will flow wet, from rocks with the same water saturations. It has often been assumed that microsphere/lepispheres (MS/LS) matrices containing water may be able to “short circuit” the resistivity measuring current. If the matrix of the opaline rock contain micro-fractures/fractures, then it is also possible that filtrate has invaded these intervals and caused an overall suppression to the resistivity response. μ -Computer tomography imaging of core plugs and good image logs would help address some of this uncertainty.

The observed MS/LS structure of opal as well as diagenesis effect from interstitial dispersed clay present with opal grains can also cause

LRLC pay. The MS/LS structure has a similar impact if distributed uniformly through the pore space; it behaves as would a laminated shale and this impacts the permeability more than the porosity. The alternating of fine-grained (clay) with coarse grained (opal MS/LS) layers means that in the former, the pore space will be saturated with formation water due to high capillary pressure, while in the latter, it will be HC saturated. From a resistivity perspective however, the resistivity response is averaged such that the overall resistivity is low. A vertical and horizontal azimuthal resistivity measurement is required to separate “sand” vs “shale” signature. If the opal mineral has macroscopic and microscopic inclusions which can result in magnetic attraction (paramagnetism), this can also cause LRLC pay, but only if found in high quantities and in electrical continuity.

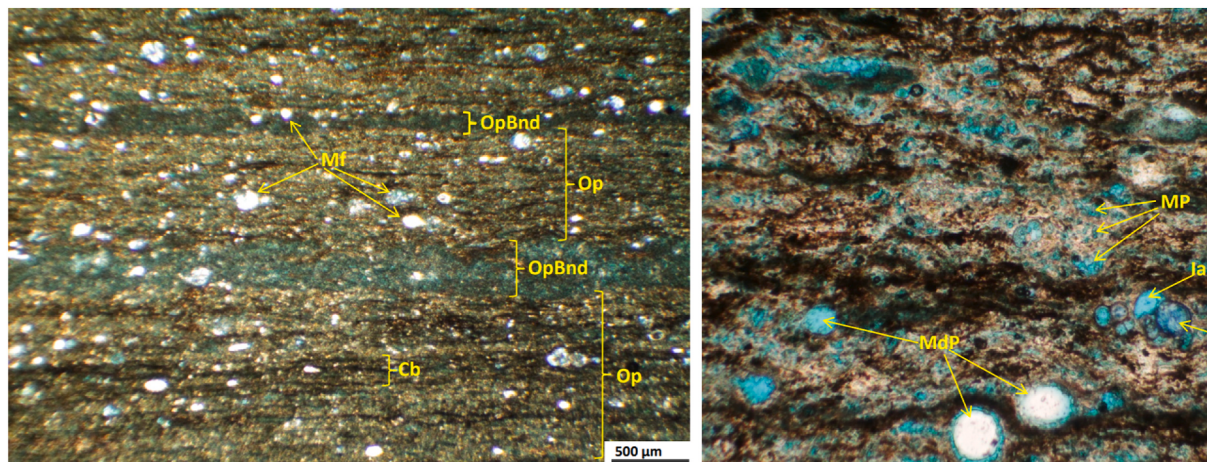


Fig. 6. Thin sections from Well DS. **Left:** Opal-rich microlaminae (Op) with intercalated bands of weakly colloform opal (OpBnd). Carbonaceous material (Cb) is also seen within microlaminae. Globular microfossils, microfossil moulds, and planktonic foraminifera are visible as bright spots throughout (Mf). **Right:** Visible matrix porosity (MP) grading to microporosity within opal matrix seen with mouldic porosity (MdP). Intraparticle porosity is hosted by a partly cemented planktonic foraminifer (IaP) partially infilled by ferroan calcite (FC). Isolated micrite trails (MtT) also observed.

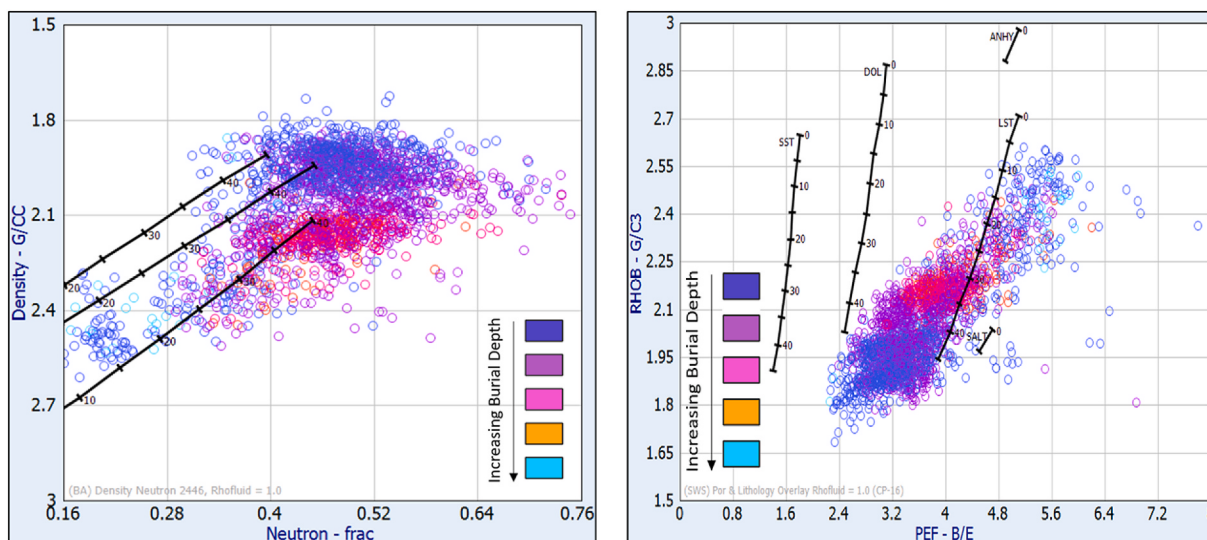


Fig. 7. Density-neutron and RHOB-PEF cross-plot.

3. Case study 2: Volcaniclastic reservoirs

3.1. Background

Volcanic tuffaceous reservoirs are known to contain hydrocarbons and have been found in significant volumes in regions such as China, Latin America, and in Indonesia, where the tuffs of the Jatibarang Field have produced over 190 MMm³ of oil and 2.7 Tcf of gas (Farooqui, et al., 2009). The great potential of these reservoirs is still relatively under-explored and underproduced, fundamentally because they are challenging to understand. As a result, tuff facies are now often ignored when encountered in conventional reservoirs, but a proper understanding of how such reservoirs behave might change that and entice the explorers looking for the next big “whale” in exploration.

The potential for hydrocarbon storage in tuffaceous reservoirs is obvious as existing reservoirs have proved they can reach good porosities of 10–25%, similar to classic sandstone reservoirs, although permeabilities are often low at <0.5 mD (Ma et al., 2016). The presence of natural fractures can increase low permeabilities by up to five orders of magnitude and further increase the reservoir potential of the tuffs (Fan

et al., 2018) and in some tight tuff reservoirs, hydraulic fracturing is necessary for commercially viable production (Ma and Huang, 2016).

However, actual reservoir quality is highly variable due to the heterogeneous nature of volcanic facies and their associated petrophysical properties. The flow mechanism in volcanic reservoirs is one such example of a property which is governed by numerous variables. Differences in pore morphology, mineralogy, and rock-fluid interactions between volcanic facies can impact reserves estimation, recovery factor, and sweep efficiency at the reservoir scale. At the pore scale, pore morphology and internal surface roughness can further affect connectivity, flow, and distribution of fluids within the reservoir (Sun et al., 2019; Wang et al., 2018).

Reservoir quality can also vary due to the level of vitrification and mineral composition, as these properties can affect alterations of pore spaces within the rock. Vitric tuffs composed dominantly of glass fragments make better reservoirs due to the higher interparticle porosity formed during alteration of glass, as opposed to crystal or lithic fragments in crystal or argillaceous tuffs (Ma, et al., 2020). Furthermore, even within similar tuff types, the composition of minerals can cause differing alkalinities between facies. Presence of more acid-soluble

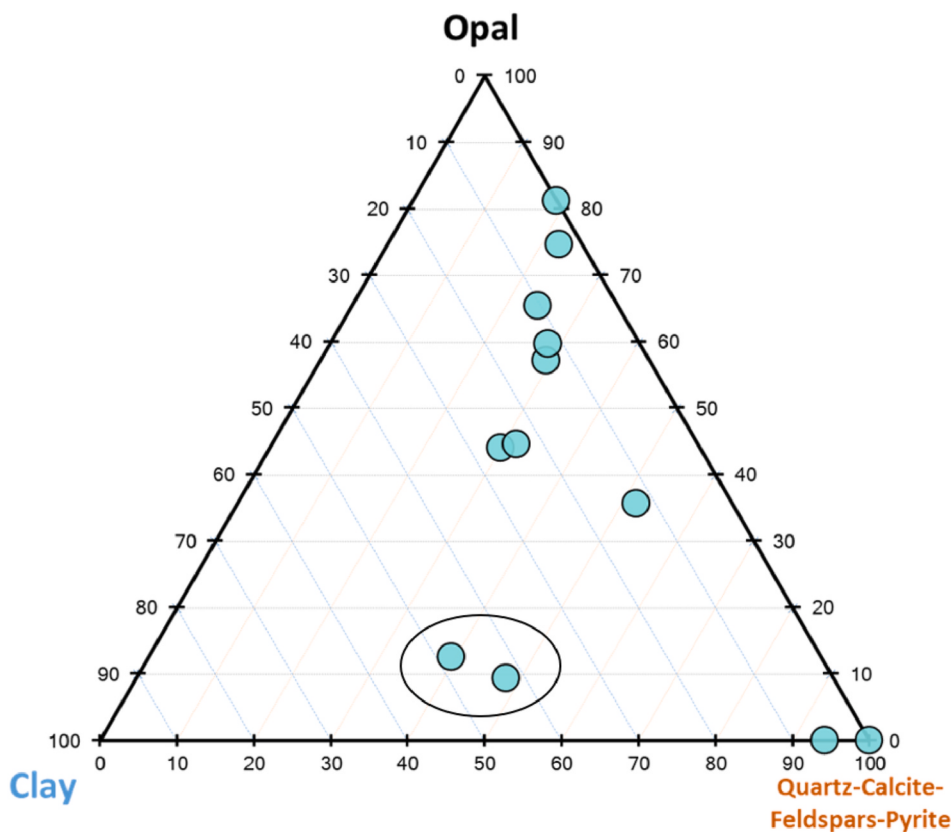


Fig. 8. Ternary plot for samples from Well DS; circled samples are identified as primarily clay rich.

minerals such as alkaline feldspars or mafic minerals can result in more alteration of the rock through chemical weathering, dissolution, or even precipitation of new minerals, all of which can affect the bulk properties of the rock (Tang et al., 2022). Tuffs may also contain trace amounts of radioactive minerals, which conventional logging methods may not work well with.

In summary, there is no generalized methodology for interpretation of volcanic reservoirs that one can follow due to the high degree of variability in volcanic facies. However, there are variables such as pore morphology, mineralogy, and rock type which are known to impact reservoir quality and potential. Analysis of these factors can be interwoven into a tailored approach to interpreting a particular volcanic reservoir, considering the specific characteristics and available data for the reservoir at hand. In the following sections we discuss our approach to examining such a well from a tuffaceous reservoir drilled in South America.

3.2. Case study parameters and setting

We will discuss Well CP in Field B, which had been logged with older “Russian style” logs, which comprised uncompensated gamma ray, neutron and resistivity logs. The well was drilled in the early 1940s, and is an onshore producer, producing prolifically for several decades. In terms of wireline data, there was no information as to the tool types, logging contractor or type of mud used. Data was available in hardcopy sephia format and had to be digitized by the operators for use in computational numerical analysis. However, because they no longer had access to the sephia or paper logs, it proved impossible to trace the vintage of these logs: there was no proper trace of when the data was digitalized, how they were digitalized, or what – if any – manipulations were made to the data. Furthermore, there was no header information to share, no information as to how the logs were calibrated, and the well had numerous vintages of neutron but it was unclear how they were

generated/corrected.

There was only a small collection of core data available in this well (mostly thin sections), but thankfully a series of core plugs from analog wells were collected from a field-wide study and measurements were made of porosity, permeability, grain density and formation factor. There were also capillary pressure measurements done using mercury, but little to no information was provided as to the sample size or dimension of the samples.

In terms of geological setting, Well CP was drilled in an onshore Tertiary-age basin with a complex geological history. The regional stratigraphy includes organic-rich carbonate platform dolomites and limestones to deep-water carbonate deposits which form the source rocks of the oil field. Later tectonic movement formed a volcanic arc which led to the deposition of andesitic and basaltic lavas and, most relevant to this study, ash and crystalline tuffs. Further collision of plate margins resulted in the deposition of synorogenic shales, conglomerates, and breccias above developing folds and other structures, forming seals.

3.3. Approach

The main challenge with the interpretation of any tuff facies is the lack of a universally accepted interpretation methodology, because of variability in the logs and fields. Indeed, it becomes necessary to design a “fit-for-purpose” method, guided by the question as to what benefit delineating the tuff facies would bring, as well as the type of data with which you must work with. For Well CP, the goal was to: (a) determine the petrophysical properties of the tuffs and (b) predict, away from well control, what the potential for hydrocarbon presence would be. For Well CP, this was even more challenging due to the presence of older “Russian style” logs.

We start our interpretation process by asking fundamental questions related to how we expect conventional logs to behave in the presence of tuffs. A silicic tuff reservoir, for instance, would have high gamma-ray

readings, due to higher thorium (Th) concentrations in felsic tuffs as noted in existing literature (Huang and Pan, 2004). Higher radioactivity could also be due to presence of potassium (K)-rich minerals, though in this sample most of the K comes in the form of plagioclase and only ^{40}K would contribute to higher gamma-ray readings (Liu et al., 2013). Electrical properties, such as resistivity, would be low, likely due to the microporous nature of the tuffs – which could also explain the higher porosity values in tuff intervals as compared to other volcanics. Densities would be potentially lower because the fine-grained mineral phase present would be distributed in a low packing density, and assuming a lack of high electron number elements, the expectation is tuffs would be like glass like material that, in general, has a low bulk density. In terms of neutron characteristics, while tuffs themselves have a low hydrogen index (HI), the intragranular porosity and large surface roughness means there can be bound/interstitial water associated with the large surface-to-volume ratio that can give high HI values. They also have low neutron capture characteristics, so in general, neutron readings can be quite high. To summarize, we would expect that typical volcanics have a “hot” gamma ray, low density, high neutron, and low resistivity signature. As will be seen in Well CP, however, this was not to be the case, primarily because of the unique output from the “Russian Logs”. In fact, we observe a low gamma ray, low neutron (count), and generally high resistivity signature.

3.4. Understanding Russian Logs

Interpreting Russian logs can be a challenge for those of us who have become accustomed to conventional modern “western” logs. Differences between the two styles are plenty: besides the use of the Cyrillic alphabet, differences in terminology, available data, and ensuing interpretation methods make employing conventional methods to interpret these unconventional logs difficult. Hence, a decent understanding of Russian logs is needed to reliably characterize a reservoir which has been measured by said tools.

Some typical measurements found in Russian logs are BKZ logs (i.e. spontaneous potential (SP), normal (PZ), lateral (GZ), and inverted lateral (GZR)) and nuclear measurements such as natural gamma-ray and neutron-gamma capture, NGK (Tingey et al., 1995). Such measurements can be made either with a single or dual detectors in wells.

Porosity is often derived from these nuclear logs, for example from neutron count rates, instead of density logs as these are rarely found for Russian logs. Depending on the type of nuclear data available and whether it is an open or cased-hole, different equations exist to compute neutron porosity values and might need to be modified for use with different datasets (Carlstrom and Cluff, 2003). Resistivity measurements from the BKZ logs can be used to compute petrophysical properties such as shale volume (VSH) and total water saturation (SWT) (Wiltgen, 1994) can be calculated from resistivity using various equations such as the Simandoux, Archie, and Indonesia equations. The use of some of these methods is covered in a later section.

3.5. Results and discussion - well CP

Besides the lack of clarity on the origins of the data and measurements from Well CP, several other issues made the analysis of this well difficult. Firstly, the already limited data set that was present was poor, with badly washed-out holes. Moreover, logs were inconsistently named, and units were not kept constant either. In intervals where lithology appeared to be consistent and cohesive, resistivity curves could swing wildly, casting a shadow of doubt on the veracity of the measurements. Even the geology of the area complicated analysis as old mudlogs described a range of rock types within the volcanic facies, which is composed primarily of basalts, or andesitic and interbed with clays, carbonates, sandstones. In some places, tuff conglomerates were intersected as well. Cuttings were also observed to have undergone severe mechanical stress under dynamic metamorphism.

Given this, we opted to follow the mantra “keep it simple” and to consider the reservoir holistically, across scales that span nine orders of magnitude. We started our analysis by firstly looking at thin sections and cores to cement our understanding of the facies, particularly the pore morphology (nm scale), before moving on to the macro properties, such as porosity-permeability and trapped residual saturation (mm to cm scale). As logging tools are not designed to measure tuff properties accurately, we applied an approach which saw us calibrating our log measurements to core on a field-wide basis (cm to m scale). To close the loop, we tied our results to the production volumes. Through this integrated approach of understanding the well at multiple scales, we could interpret the petrophysical properties to a reasonable degree of confidence.

3.6. Thin section, Scanning Electron Microscope and core

An analysis of the thin sections of the tuffaceous facies showed characteristic needle fragments of volcanic origin along with a series of heterogeneous pore sizes, and complex mineralogy (albite, polycrystalline quartz, fine grained plagioclase, carbonates and abundant detrital clay matrix). Tuff is complicated because it is hard to define/separate macro/meso/micro porosity, primarily due to (a) surface roughness and (b) no clear boundary in pore sizes, but from Fig. 9 we can observe qualitatively that the pore space is made up of a distribution of macropores and micropores with mesopores acting to bridge the two other pore types. We observed that the micropores are in connection (blue filled space) while there are clay present in macropore, and which itself appears isolated (labeled as ‘A’ in the image). We also observed there to be calcite-filled flow channels present within fractures in the rock. These fractures are possibly an indirect indication of the brittle nature of the tuff rock.

Mercury intrusion capillary porosimetry (MICP) measured on 2 cuttings samples showed pore sizes ranging from $0.0125\ \mu\text{m}$ to $7.5\ \mu\text{m}$. These pore sizes were plotted on a simplified cumulative distribution plot (Fig. 10) based on MICP plots used by Abuamarah and Nabawy (2021) for reservoir characterization, though in this case we use the plot simply to visualize pore size distribution between our two samples. While both sample 1 and sample 2 were taken within 5 m of one another within a producing zone, both samples showed dissimilar pore-size distributions, with sample 2 having significantly more microporosity. This only highlights the heterogeneity present within volcanics. While the heterogeneity and sparsity of samples makes it impossible to properly differentiate between macro, meso and micropores, we “crudely” classify the pore size distribution into micropores with pore radii $<0.04\ \mu\text{m}$ and macropores with pore radii $>1.4\ \mu\text{m}$. We base this classification on work by Ma and Huang (2016), where, in the 58 tuff samples they analyzed, the maximum pore throat radii ranged from $0.003\ \mu\text{m}$ to $0.835\ \mu\text{m}$. Note that tuffs have much smaller pore radii than conventional oil and gas reservoirs elsewhere (Nabawy et al., 2009).

We view sample 1 as being more representative of the “typical” hydrocarbon bearing reservoir, if only based on the pore size distribution, where $\sim 59\%$ of the pore volume is associated with the macroporosity while $\sim 18\%$ of the sample is microporosity. With sample 2, we note the distribution to be reversed, with $\sim 11\%$ of the sample being macroporous while $\sim 82\%$ of the pore space can be defined as microporous. This sample could potentially be representative of the more “typical” baffle seen in heterogeneous reservoir.

3.7. Core calibrated porosity-permeability trends

Vintage core data described the tuffaceous facies as being either coarse, medium, or fine grained. This classification is general, however, and there was no mention in the data of how this definition was determined. Adding to the confusion was that no indication was given as to whether porosity was total or effective, despite there being mention in the core reports of cores being oven dried as part of the porosity

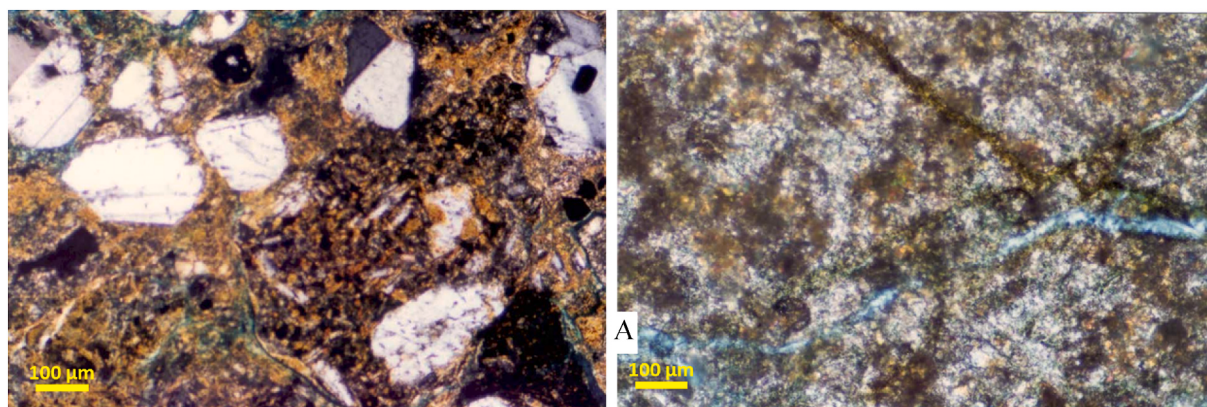


Fig. 9. Thin section images of volcanoclastic sample.

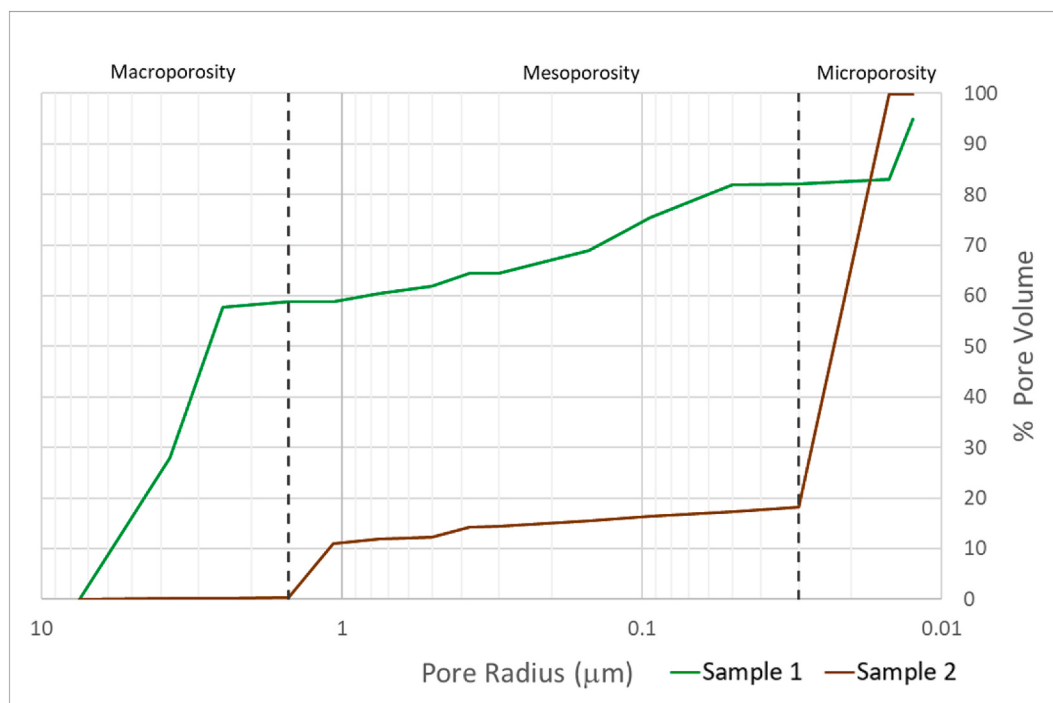


Fig. 10. Pore size distribution from MICP

measurement process. We thus assumed that porosity referred to here is total porosity. If all the data is plotted in the form of a Rock Quality Index (RQI) against normalized porosity, one observes that three are clear separation of the core into three distinct groups Fig. 11 (b). It can be generally observed that, for the same porosity value, coarse grained tuffs have a higher RQI in contrast to the fine-grained material. Additionally, the data is highly scattered, with some pockets of fine-grained tuffs having very high RQI values. Again, this alludes to the highly heterogeneous nature of the volcanic facies. Rock typing using other methods such as those outlined in El Sawy et al. (2020) can help improve the characterization of such heterogenous reservoirs. Still, the range of values (for this field) has a majority of the samples from 5 to 32 p.u with permeability ranging from 0.1 to 100 mD (Fig. 11 (a)).

3.8. XRD mineralogy

As seen in Fig. 12, most tuff samples are dominantly made of quartz, plagioclase, and feldspar, with clay as the second largest component which makes up about a quarter of all components within the tuffs on

average. Cement is the least abundant component and is likely found within healed fractures. The relatively high content of ductile and highly plastic clay suggests that natural open fractures are less likely to be found within the rock (Guo, et al., 2015; Ma et al., 2019), and further hydraulic fracturing might be needed to increase production from such a formation. Existing hydrocarbon fluids would likely be contained within the macroporosity supported by framework grains and could possibly fill the micropore spaces as well, given the extensive proportion of microporosity. However, this would depend on factors such as the column height.

3.9. Trapped gas saturation

The well is a hydrocarbon producer, with no produced water, and has been in production for decades. This unusual production profile was confirmed when a series of experiments were conducted on core, to measure the trapped phase saturation as a function of the core porosity. Given in Fig. 13 (left) is the behavior of the core samples, contrasted against samples from literature (tight sands, shaly sands, and clean

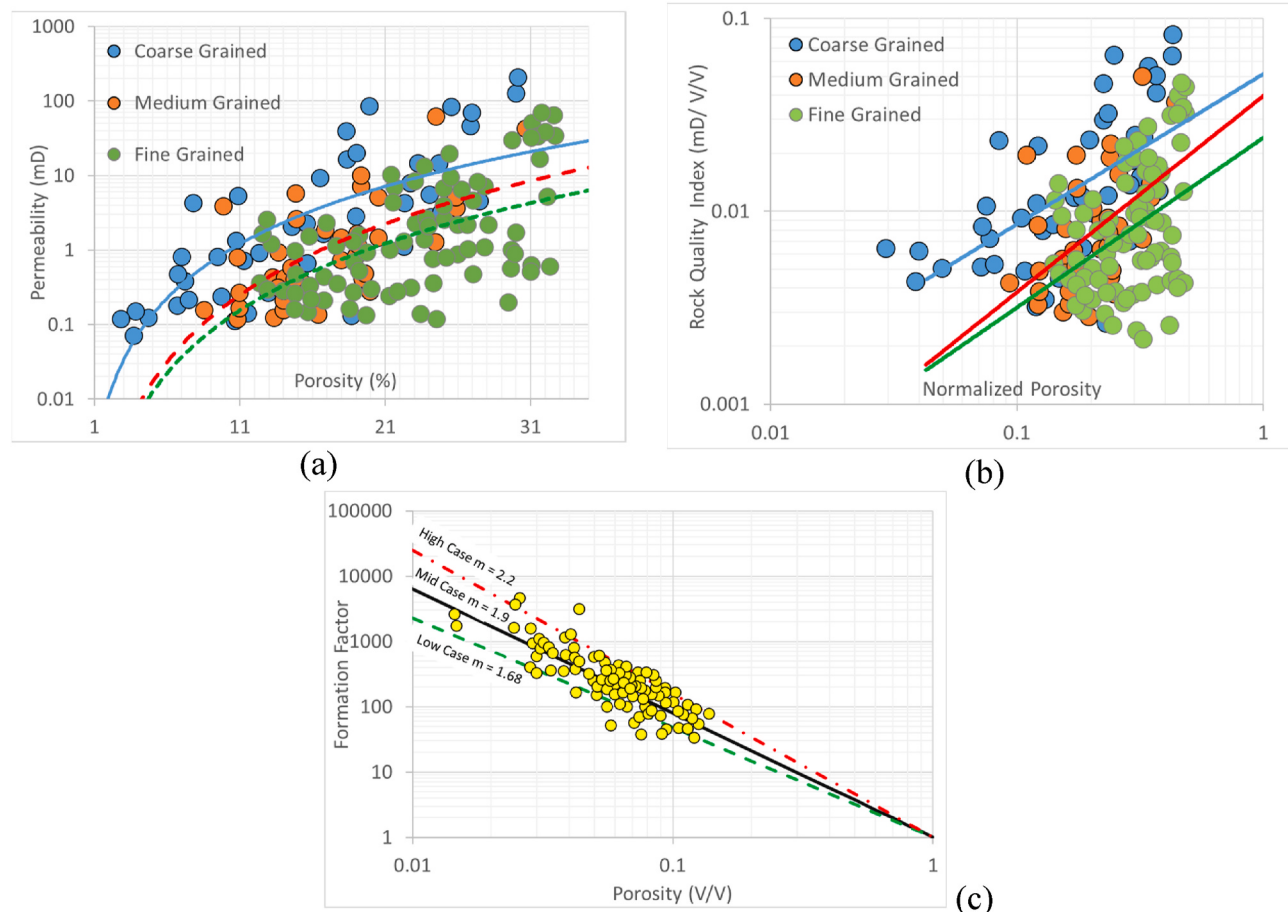


Fig. 11. Generic Petrophysical Properties of volcanoclastic rock (a) Porosity-Permeability trend, (b) Rock quality index (RQI) against normalized porosity, and (c) Formation volume factor against porosity. This utilizes formula $F = a\Phi^{-m}$, where $m = 1.68, 1.9$, and 2.2 for the low, mid, and high cases respectively, while $a = 1$ for all cases.

reservoir core, which have little to no clay). Fig. 13 (left) indicated that volcanic type facies are capable of very low irreducible saturations, with higher porosity samples having a slightly higher irreducible phase.

We attribute this to the unique pore geometry such volcanoclastic sediments possess. As seen from the thin sections, the pore space is made up of thin lenticular pore-throats (Fig. 9). While sample 1 in Fig. 10 shows the macropore space to be $\sim 59\%$ of the pore volume, there is a large range of mesopores sizes taking up $\sim 23\%$ of the pore volume and which span $\sim 0.05\text{--}1 \mu\text{m}$ radius, and which act to connect the macroporosity. We illustrate the thin lenticular-type pore-throats in Fig. 13 (right) and label it “Pore-throat type A”.

When oil is produced, water imbibes into the vacated pore space. The imbibition of a wetting fluid into a porous reservoir is influenced by rate, heterogeneity of the pore space and local pore geometry, which can lead to a wide variety of wetting patterns and hence a diversity in oil trapping (Wang et al., 2016). Here, we think that the low aspect ratio (ratio of pore-to-throat radii) and the fact that the system is so well connected, with very little occluded porosity (high coordination numbers) puts the volcanic sample in the realm of a flat, slow flood front, with very little to no water film ahead of the invading water. This prevents snap-off of oil from occurring and thus a low residual oil saturation (Kumar, 2009).

3.10. Petrophysical evaluation

Fig. 14 shows the input logs (pre-production) and the final interpretation result. We have renamed some of the logs to a more familiar “western” style name, for convenience. The left-most track shows the spectral GR (SGR) log as well as the caliper (CALI) and SP log. From

these logs, we observe that the SGR has a very limited dynamic range, with SGR ranging from 2 to 5 GAPI. Given the vintage of the logs, no information was available on the K, Th, or U constituents. We note the condition of the borehole, with quite a bit of rugosity as evidenced by the washouts in the CALI log. Finally, while there is an SP log, it too showed no variation throughout. While an attempt was made to utilize the SP log for saturation or VSH evaluation, this was abandoned as (a) there was no information regarding the mud properties used in the well, and (b) there was no clearly definable “shale” that could be used for a baseline.

We instead interpreted VSH from the deepest resistivity reading (RESDEEP¹), given in track 3 from the left. From the logs in Fig. 14, we observe that there is a fair amount of variation in the log. We assume that the resistivity log reads deep enough (at least over 30 inches) into the formation to be unaffected/marginally affected by any washout (Frenkel et al., 1997). We subsequently note at depth Y40 that there is a low resistivity value which we attribute to the presence of clay/shale, and which we use for our “shale”² baseline –We then apply Eq. (1) to determine the VSH volume:

¹ We assumed the normal PZ log, with short spacings of 0.25–0.5 m, to be equivalent to the medium resistivity (RESMED), while the lateral GZ log, with spacing up to 1 m, to be equivalent to the deep resistivity (RESDEEP).

² Note that “shale” here refers to a shaly claystone that we have used as a shale equivalent.

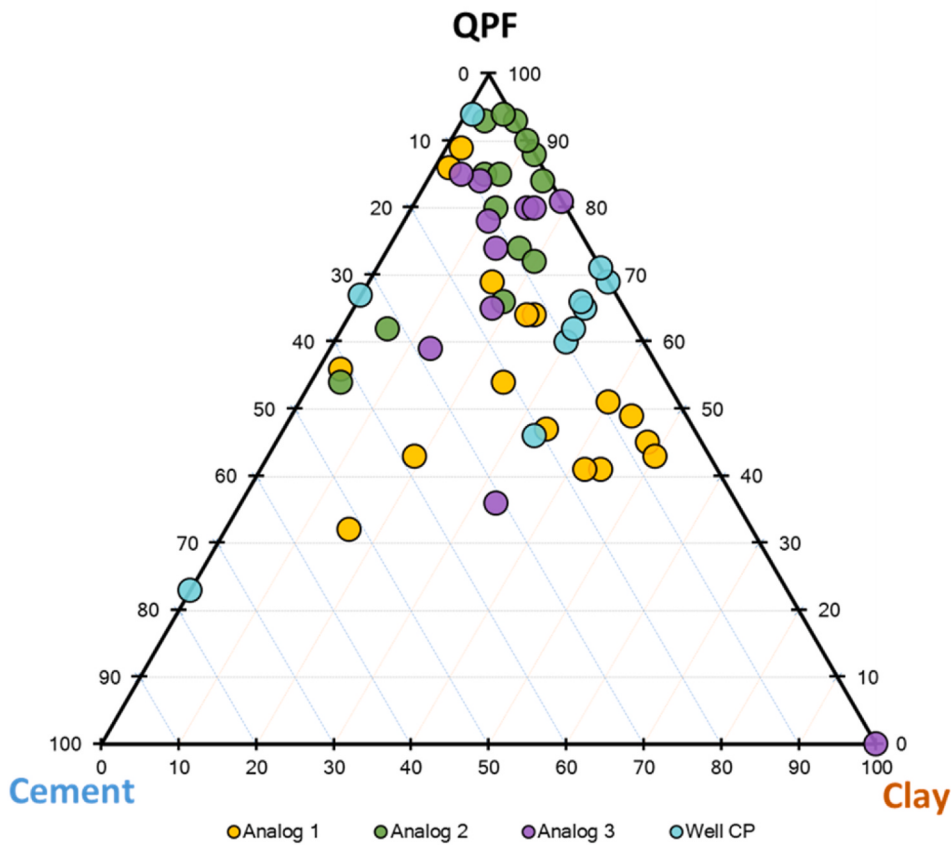


Fig. 12. Ternary plot for samples from Well CP and other analog wells within the field. QPF refers to quartz, plagioclase, and feldspar.

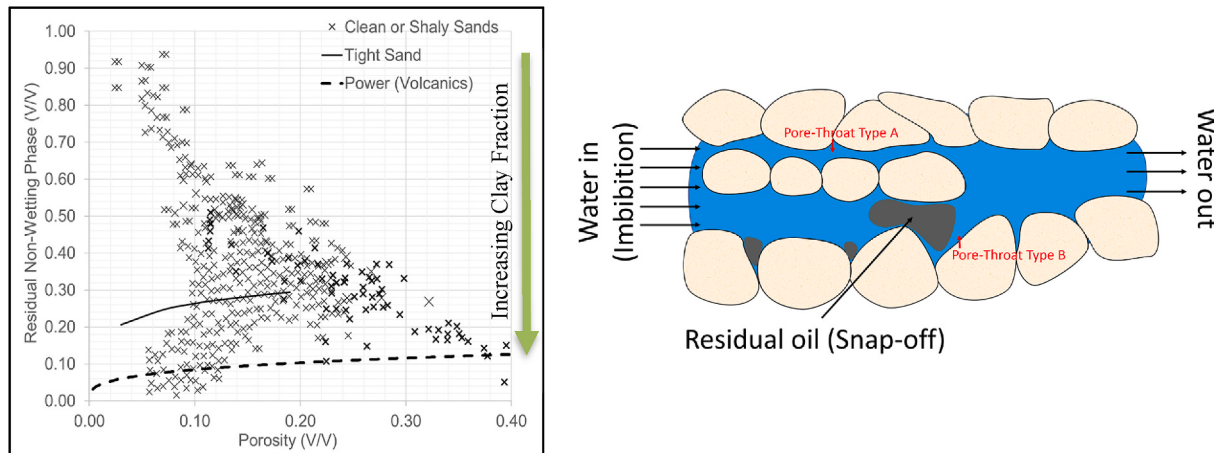


Fig. 13. **Left:** A comparison of the trapped residual phase saturation as a function of porosity between the volcanic rocks and other rock types. Adapted from Hamon et al. (2001) and Jiang et al. (2021). **Right:** schematic of the sweep mechanism present in volcanic rock, where pore throat type A is likely to dominate more than pore throat type B.

$$\text{VSH from Resistivity VSH} = \left[\frac{R_{sh}(R_{lim} - R_t)}{R_t(R_{lim} - R_{sh})} \right]^{1/b} \quad 1$$

where R_{sh} is the resistivity of the shale (ohmm), R_{lim} is the maximum resistivity in clean pay intervals (ohmm), R_t is resistivity measured on logs (ohmm) and $b = 1.0\text{--}2.0$ [dimensionless] (Poupon and Gaymard, 1970). The results are displayed on the log plot as the first log on the right.

We had initially intended to evaluate total porosity (PHIT) using both near and far counts measured by the neutron log (NEAR and FAR),

as no density log is present. These logs were present in other wells in Field B. Unfortunately, there was only NEAR counts present for Well CP. We instead converted the NEAR counts to an "estimated" neutron porosity (PHIN), utilizing an old chart book correlation, as given in Fig. 15. Typically, for such correlation to be accurate, information about the type of tool is needed, but this information was not available for this well, and thus, the correlation was applied assuming a generic NGK style tool from the 1950s.

To reduce the uncertainty with having to estimate "estimate" PHIN, we applied a "high-low" correlation to the log, where high and low PHIN

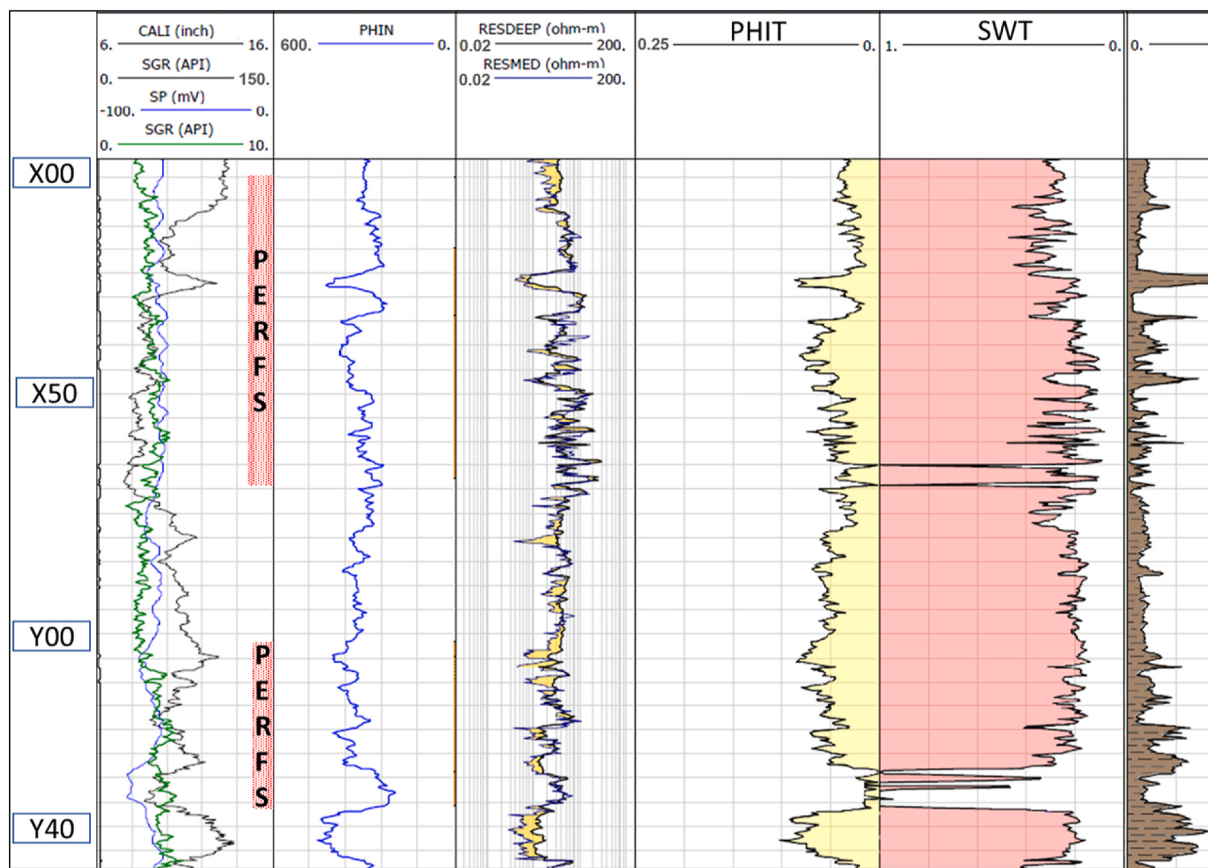


Fig. 14. Log data and interpretation for well CP.

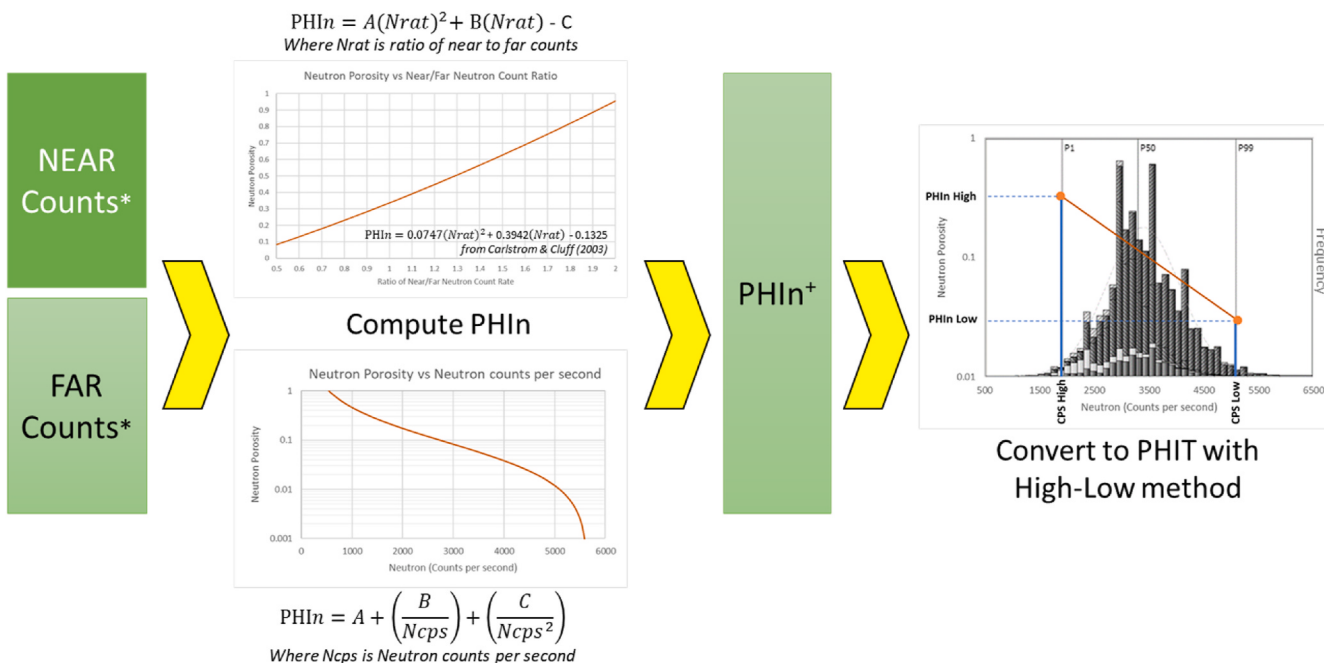


Fig. 15. Workflow applied in volcanic log interpretation.

values are calibrated to core based end-points (Figs. 11 (a) and Fig. 15). We assumed that low counts/high PHIN was equivalent to high porosity and vice-versa. We independently cross checked the results of the interpretation with field wide core data, to determine if we are within

the expected range of values.

$$\text{PHIn from NEAR counts } \text{PHIn} = A + \left(\frac{B}{N_{\text{cps}}} \right) + \left(\frac{C}{N_{\text{cps}}^2} \right)$$

SWT is interpreted using the modified Indonesia equation (Eq. 4) and compared it to the Archie method (Eq. (3)). We used the Indonesia equation to account for the potential effect of the clays. We observed that both results appear similar, and only show the result of the Indonesia equation in the log plot (second track from the right). The equations applied are:

$$\text{Archie} \quad 3 \\ \text{model } S_w^n = \frac{aR_w}{\phi^m R_t}$$

$$\text{Indonesia} \quad 4 \\ \text{model } \frac{1}{\sqrt{R_t}} = \left[\frac{VSH^{(1-\frac{n}{2})}}{\sqrt{R_{sh}}} + \frac{\phi^{m/2}}{\sqrt{aR_w}} \right] \times SWT^{\frac{n}{2}}$$

where SWT is total water saturation (V/V), R_w is the resistivity of the formation water (ohmm), m is the porosity exponent [dimensionless], n is the saturation exponent [dimensionless], a is the tortuosity factor [dimensionless] and ϕ (=PHIT) is the total porosity (V/V).

As alluded to earlier, there was no produced water in this well, so salinity could only be determined from regional analogs. For this well, we determined that a salinity value of ~90,000 ppm NaCl equivalent to be reasonable from the information we could gather, with $a = 1$ and $m \sim 2$ from the core data in Fig. 11 (c). As there is no n data, we assume that both m and n are equal. Temperature was determined from temperature measured by production logs.

Interestingly, we note the very high saturation values being interpreted. While we definitively cannot exclude the possibility that the salinity value we have used is incorrect, we are confident that there is movable hydrocarbons present in this interval. Additionally, we are cognizant that the wireline logs were acquired pre-production. Indeed, when we checked the results against production information, we have found that the intervals marked "PERFS" are still producing oil 50–100 bopd currently, with a cumulative production of >500 Mstb, giving us confidence in our interpretation. We also noted that zones where RESDEEP and medium resistivity (RESMED) logs showed a separation were the most prolific production zones. In these zones, we viewed the separation as indicative of permeability presence, which we viewed as a proxy for producibility.

4. Limitations of study

This study is limited by the fact that in both our case studies, we only had a limited amount of data which intersected these unique mineralogies. As such, while our interpretations and analysis are valid and useful for the exact lithologies and compositions of rocks that we have worked with, they may not necessarily be fully applicable to all other rocks containing these unique mineralogies considering the possible variations in microstructure, composition, and grain size. More data on unique mineralogy will give us a better idea of the range of petrophysical effects we can expect to see within these rocks. We instead recommend that interpretation methods be developed from first principles and tailored to the available data and geology of the area.

5. Conclusions

Analysis of both of our case studies show that while opalines and tuffaceous reservoirs are uncommon and hence not typically associated with reservoir potential, the unique microstructures found in both wells indicate that they do in fact have potential to store hydrocarbons. With the opaline Well DS, there were hydrocarbon traces, while with the volcanic Well CP is a prolific producer.

In opalines, opal-CT MS/LS create a microporous structure that could potentially store fluids. Opalines can be fracture or matrix-porosity dominated, and both allow hydrocarbons to be stored within the rocks, although through different means. Hence, we hypothesize that

opalines can be classified as LRLC pay and should not be ignored simply because typical hydrocarbon markers do not show up on logs. In tuffs and volcanics, the heterogeneity of pore sizes means increased connectivity. We also observe that dominantly thin and laminated pore geometry reduces residual oil within the rock. Petrophysical interpretations of old Russian style logs showed high saturation values, confirmed by high hydrocarbon production within the intervals of interpreted high saturation. Furthermore, we note that bigger separations between deep and medium resistivity curves coincide with intervals of high production, suggesting that this can be used as a proxy for producibility.

Funding sources

This research did not receive any specific grant from funding agencies in the public, commercial, or not-for-profit sectors.

Declaration of competing interest

The authors declare that they have no known competing financial interests or personal relationships that could have appeared to influence the work reported in this paper.

Data availability

The data that has been used is confidential.

Acknowledgments

We would like to thank Maria Irene Inggrid for peer review of this work.

Abbreviations

bopd	barrels of oil per day
CALI	caliper
CPI	computer processed interpretation
D-N	neutron density
DRHO	bulk density correction
g/cc	gram per cubic centimetre
GAPI	gamma-ray (American petroleum industry) units
GR	gamma-ray
GRV	gross rock volume
K	potassium
LRLC	low resistivity low contrast
m	metre
M & MM	thousands and millions respectively
mD	millidarcy
MICP	mercury intrusion capillary porosimetry
mMD	measured depth in metres
MS/LS	microspheres/lepispheres
NGK	neutron-gamma capture; in Russian-style logs
NPHI	density-neutron
ohmm	ohm metres
PEF	bulk photoelectric effect
PHIE	effective porosity
PHIT	total porosity
RES	resistivity
RESDEEP	deep resistivity
RESMED	medium resistivity
RHOB	bulk density
RHOGC	grain density
SGR	spectral gamma-ray
SP	spontaneous potential
stb	stock tank barrel (42 US gallons measured at 14.7 pounds per square inch and 60 °F)

Sw	saturation of water
SWE	effective water saturation
SWT	total water saturation
Tcf	trillion cubic feet
Th	thorium
U	uranium
VCL	volume of clay
VSH	volume of shale
XRD	X-Ray Diffraction
ϕ	porosity

References

- Ali Ali, E., Emad El Din Abd Elrazik, E., Shebl Azam, S., Ahmed Hassan, S., 2016. Integrated petrophysical and Lithofacies studies of lower-middle Miocene reservoirs in Belayim marine oil field, Gulf of Suez, Egypt. *J. Afr. Earth Sci.* 117, 331–344.
- Abuamarah, B.A., Nabawy, B.S., 2021. A proposed classification for the reservoir quality assessment of hydrocarbon-bearing sandstone and carbonate reservoirs: a correlative study based on different assessment petrophysical procedures. *J. Nat. Gas Sci. Eng.* 88, 103807 <https://doi.org/10.1016/j.jngse.2021.103807>. Retrieved from.
- Armelentzi, G., Goldberg, K., Alvarenga, R., Kuchle, J., Amarante, F.B., Scherer, C.M., De Ros, L.F., 2021. Depositional and diagenetic impacts on the porosity of post-salt carbonate reservoirs of southern Campos Basin, southeastern Brazilian margin. *J. S. Am. Earth Sci.* 112 (1).
- Ashqar, A.U., 2016. Evaluating a Complex Low Resistivity Pay Carbonate Reservoir Onshore Abu Dhabi: from Model to Implementation. Society of Petroleum Engineers, pp. 1–14. Paper No 182912-MS.
- Ayadiuno, C.B., 2017. Investigating Low Resistivity Low Contrast Resistivity Pay in a Permo-Carboniferous Reservoir, Central Saudi Arabia. Society of Petroleum Engineers, pp. 1–17. Paper No 188887-MS.
- Baouche, R., Nabawy, B.S., 2021. Permeability prediction in argillaceous sandstone reservoirs using fuzzy logic analysis: a case study of triassic sequences, Southern Hassi R'Mel Gas Field, Algeria. *J. Afr. Earth Sci.* 173, 104049 <https://doi.org/10.1016/j.jafrearsci.2020.104049>. Retrieved from.
- Belevich, A., 2017. The Problem with Silt in Low Resistivity Low Contrast Pay Reservoirs. Society of Petrophysicists and Well-Log Analysts, pp. 1–19.
- Boyd, A., Darling, H., Tabanou, J., 1995. The lowdown on low resistivity pay. *Oilfield Rev.* 7, 7–14.
- Carlstrom, G.M., Cluff, R.M., 2003. Western analysis of Russian log data. In: SPWLA 44th Annual Logging Symposium. OnePetro, Galveston, Texas.
- Chaika, C., Dvorkin, J., 2000. Porosity reduction during diagenesis of diatomaceous rocks. *AAPG (Am. Assoc. Pet. Geol.) Bull.* 84 (8), 1173–1184. <https://doi.org/10.1306/A9673C70-1738-11D7-8645000102C1865D>. Retrieved from.
- Chaika, C., Williams, L.A., 2001. Density and mineralogy variations as a function of porosity in miocene Monterey Formation oil and gas reservoirs in California. *AAPG (Am. Assoc. Pet. Geol.) Bull.* 85 (1), 149–167. <https://doi.org/10.1306/8626C785-173B-11D7-8645000102C1865D>. Retrieved from.
- Clavier, C., Heim, A., Scala, C., 1976. Effect of pyrite on resistivity and other logging measurements. Society of Petrophysicists and Well Log Analysts 17th Annual Symposium 1–34.
- Curtis, N.J., Gascooke, J.R., Johnston, M.R., Pring, A., 2019. A review of the classification of opal with reference to recent new localities. *Minerals* 9 (5), 299.
- Derkowski, A., Środon, J., McCarty, D.K., 2015. Cation exchange capacity and water content of opal in sedimentary basins: example from the Monterey Formation, California. *Am. Mineral.* 100 (5–6), 1244–1256. <https://doi.org/10.2138/am-2015-5008>. Retrieved from.
- Dietrich, J.K., 2017. Heavy oil recovery from opal-CT diatomite. In: SPE Western Regional Meeting, April 2017. Bakersfield, California. <https://doi.org/10.2118/185686-MS>. Retrieved from.
- El Sawy, M.Z., Abuhagaza, A.A., Nabawy, B.S., Lashin, A., 2020. Rock typing and hydraulic flow units as a successful tool for reservoir characterization of Bentiu-Abu Gabra sequence, Muglad basin, southwest Sudan. *J. Afr. Earth Sci.* 171, 103961 <https://doi.org/10.1016/j.jafrearsci.2020.103961>. Retrieved from.
- Ellis, G.K., 2016. The North Rankin Gas Field, Carnarvon Basin, Australia—Late Authigenic Pyrite Evidence of Early Oil Entrapment and Oil-Charged Fluid Flow. Society of Exploration Geophysicists Global Meeting Abstracts, pp. 1–6.
- Fan, C., Qin, Q., Liang, F., Fan, Z., Li, Z., 2018. Fractures in volcanic reservoirs: a case study in zhongguai area at the northwestern margin of junggar basin (China). *Earth Sci. Res.* 22 (3), 169–174.
- Farooqui, M.Y., Hou, H., Li, G., Machin, N., Neville, T., Pal, A., Yang, X., 2009. Evaluating volcanic reservoirs. *Oilfield Rev.* 21 (1), 36–47.
- Feng, Y.W., Ren, Y., Zhang, G.C., Qu, H.J., 2020. Petroleum geology and exploration direction of gas province in deepwater area of North Carnarvon Basin, Australia. *China Geology* 3 (4), 623–632.
- Fredrich, J.T., Fossum, A.F., Hickman, R.J., 2007. Mineralogy of deepwater Gulf of Mexico salt formations and implications for constitutive behavior. *J. Petrol. Sci. Eng.* 57, 354–374.
- Frenkel, M.A., Mezzatesta, A., Strack, K., 1997. Enhanced interpretation of Russian and old electrical resistivity logs using modeling and inversion methods. In: SPE Annual Technical Conference and Exhibition. OnePetro, San Antonio, Texas. Retrieved from SPE Annual Technical Conference and Exhibition.
- Guo, J.-C., Luo, B., Zhu, H.-Y., Wang, Y.-H., Lu, Q.-L., Zhao, X., 2015. Evaluation of fracability and screening of perforation interval for tight sandstone gas reservoir in western Sichuan Basin. *J. Nat. Gas Sci. Eng.* 25, 77–87.
- Hamon, G., Suzanne, K., Billiotte, J., Trocmé, V., 2001. Field-wide variations of trapped gas saturation in heterogeneous sandstone reservoirs. In: SPE Annual Technical Conference and Exhibition. OnePetro, New Orleans, Louisiana. <https://doi.org/10.2118/71524-MS>. Retrieved from.
- Huang, B., Pan, B., 2004. Characteristics of log responses and lithology determination of igneous rock reservoirs. *J. Geophys. Eng.* 1 (1), 51–55.
- Jiang, Z., Fu, J., Li, G., Mao, Z., Zhao, P., 2021. Using resistivity data to study the waterflooding process: a case study in tight sandstone reservoirs of the Ordos Basin, China. *Geophysics* 86 (2), B55–B65. <https://doi.org/10.1190/geo2020-0401.1>. Retrieved from.
- Jones, J.B., Segnit, E.R., 1971. The nature of opal I. nomenclature and constituent phases. *J. Geol. Soc. Aust.* 18 (1), 57–68. <https://doi.org/10.1080/00167617108728743>. Retrieved from.
- Jong, J., Kessler, F.L., Madon, M., Mohamad, H., 2019. Radioactive apatite-rich "Hot Sands" of the Tenggol Arch: stratigraphic curiosity or sub-seismic reservoir correlation tool? *Bull. Geol. Soc. Malays.* 67, 1–10.
- Kennedy, M.C., 2004. Gold fool's: detecting, quantifying and accounting for the effects of pyrite on modern logs. Society of Petrophysicists and Well Log Analysts 45th Annual Logging Symposium 1–12.
- Kumar, M., 2009. Multiphase Flow in Reservoir Cores Using Digital Core Analysis. Canberra. PhD Thesis. Australian National University.
- Liu, H., Li, X., Liao, J., Liu, X., 2013. Genesis of the high gamma sandstone of the yanchang formation in the ordos basin, China. *Petrol. Sci.* 10, 50–54.
- Ma, C., Dong, C., Lin, C., Elsworth, D., Luan, G., Sun, X., Liu, X., 2019. Influencing factors and fracability of lacustrine shale oil reservoirs. *Mar. Petrol. Geol.* 110, 463–471.
- Ma, J., Huang, Z., 2016. Tight-reservoir micropore formation and evolution in sedimentary organic-matter-bearing tuff: a case study from the Permian Tiaohu Formation in the Santanghu Basin, NW China. *Aust. J. Earth Sci.* 63 (4), 485–501.
- Ma, J., Huang, Z., Liang, S., Liu, Z., Liang, H., 2016. Geochemical and tight reservoir characteristics of sedimentary organic-matter-bearing tuff from the Permian Tiaohu formation in the santanghu basin, northwest China. *Mar. Petrol. Geol.* 73, 405–418.
- Ma, J., Liu, G., Huang, Z., Ou, G., Li, T., Guo, X., 2020. Tight tuff reservoir characteristics and its controlling factors: a comparative study of the Permian Tiaohu formation and carboniferous Haerjiawu formation in the santanghu basin, NW China. *J. Petrol. Sci. Eng.* 187, 106808.
- Marisa, R.B., Anger, B., Hertel, S., Dietderich, J., Patino, J., Appel, M., 2018. Investigation of salt-bearing sediments through digital rock Technology Together with experimental core analysis. *Petrophysics* 59 (1), 1–12.
- Nabawy, B.S., Géraud, Y., Rochette, P., Bur, N., 2009. Pore-throat characterization in highly porous and permeable sandstones. AAPG (Am. Assoc. Pet. Geol.) Bull. 93 (6), 719–739.
- Nabawy, B.S., Lashin, A.A., Barakat, M.K., 2022. Implementation of lithofacies and microfacies types on reservoir quality and heterogeneity of the late cretaceous Upper Bahariya member in the shurouk field, shoushan basin, north western desert, Egypt. *J. Asian Earth Sci.* 224, 105014 <https://doi.org/10.1016/j.jseaes.2021.105014>. Retrieved from.
- Poupon, A., Gaymard, R., 1970. The evaluation of clay content from logs. In: SPWLA 11th Annual Logging Symposium.
- Pratama, E., Ismail, M.S., Ridha, S., 2017. An integrated workflow to characterize and evaluate low resistivity pay and its phenomenon in a sandstone reservoir. *J. Geophys. Eng.* 14 (3), 513–519. <https://doi.org/10.1088/1742-2140/aa5efb>. Retrieved from.
- Radwan, A.A., Nabawy, B.S., Abdelmaksoud, A., Lashin, A., 2021. Integrated sedimentological and petrophysical characterization for clastic reservoirs: a case study from New Zealand. *J. Nat. Gas Sci. Eng.* 88, 103797 <https://doi.org/10.1016/j.jngse.2021.103797>. Retrieved from.
- Reid, S.A., McIntyre, J.L., 2001. Monterey Formation porcelainite reservoirs of the Elk Hills field, kern county, California. *AAPG (Am. Assoc. Pet. Geol.) Bull.* 85 (1), 169–189. <https://doi.org/10.1306/8626C78F-173B-11D7-8645000102C1865D>. Retrieved from.
- Saxena, V., McDonald, T., 2009. Exploration Petrophysics for intra-salt carbonate in Ultra saline environment. International Petroleum Technology Conference 13332, 1–14.
- Sun, H., Zhong, D., Zhan, W., 2019. Reservoir characteristics in the Cretaceous volcanic rocks of Songliao Basin, China: a case of dynamics and evolution of the volcano-porosity and diagenesis. *Energy Explor. Exploit.* 37 (2), 607–625.
- Tang, H., Tian, Z., Gao, Y., Dai, X., 2022. Review of volcanic reservoir geology in China. *Earth Sci. Rev.* 232, 104158.
- Tingeay, J.C., Nelson, R.J., Newsham, K.F., 1995. Comprehensive analysis of Russian petrophysical measurements. In: SPWLA 36th Annual Logging Symposium. OnePetro, Paris, France.
- Tsuji, T., Masui, Y., Yokoi, S., 2011. New hydrocarbon trap models for the diagenetic transformation of opal-CT to quartz in Neogene siliceous rocks. *AAPG (Am. Assoc. Pet. Geol.) Bull.* 95 (3), 449–477. <https://doi.org/10.1306/06301009192>. Retrieved from.
- Wang, S., Tokunaga, T.K., Wan, J., Dong, W., Kim, Y., 2016. Capillary pressure-saturation relations in quartz and carbonate sands: limitations for correlating capillary and wettability influences on air, oil, and supercritical CO₂ trapping. *Water Resour. Res.* 52 (8), 6671–6690. <https://doi.org/10.1002/2016WR018816>. Retrieved from.
- Wang, W., Wang, Z., Chen, X., Long, F., Lu, S., Liu, G., Su, Y., 2018. Fractal nature of porosity in volcanic tight reservoirs of the Santanghu basin and its relationship to pore formation processes. *Fractals* 26 (2), 184007.

- Wiltgen, N.A., 1994. The essential of basic Russian well logs and analysis techniques. In: SPWLA 35th Annual Logging Symposium. OnePetro, Tulsa, Oklahoma.
- Winardi, S., Surjono, S.S., Amijaya, D.H., Suryanto, W., 2021. Reservoirs resistivity correction factor in low resistivity pyritic sandstone reservoirs. International Conference on Geological Engineering and Geosciences 851, 1–11.
- Worthington, P., 2000. Recognition and evaluation of low resistivity pay. Petrol. Geosci. 6, 77–92.